



## RESEARCH ARTICLE

10.1002/2015PA002849

## Key Points:

- Ocean surface conditions were reconstructed from the SE Greenland shelf for the last millennium
- The Medieval Climate Anomaly 1000 to 1200 C.E. represents the warmest period of the late Holocene
- Solar forcing amplified by atmospheric forcing was behind the surface conditions

## Supporting Information:

- Figures S1–S5

## Correspondence to:

A. Miettinen,  
arto.miettinen@npolar.no

## Citation:

Miettinen, A., D. V. Divine, K. Husum, N. Koç, and A. Jennings (2015), Exceptional ocean surface conditions on the SE Greenland shelf during the Medieval Climate Anomaly, *Paleoceanography*, 30, 1657–1674, doi:10.1002/2015PA002849.

Received 23 JUN 2015

Accepted 26 NOV 2015

Accepted article online 2 DEC 2015

Published online 26 DEC 2015

## Exceptional ocean surface conditions on the SE Greenland shelf during the Medieval Climate Anomaly

Arto Miettinen<sup>1</sup>, Dmitry V. Divine<sup>1,2</sup>, Katrine Husum<sup>1</sup>, Nalan Koç<sup>1</sup>, and Anne Jennings<sup>3</sup>

<sup>1</sup>Norwegian Polar Institute, Tromsø, Norway, <sup>2</sup>Department of Mathematics and Statistics, Arctic University of Norway, Tromsø, Norway, <sup>3</sup>INSTAAR and Department of Geological Sciences, University of Colorado Boulder, Boulder, Colorado, USA

**Abstract** Diatom inferred 2900 year long records of August sea surface temperature (aSST) and April sea ice concentration (aSIC) are generated from a marine sediment core from the SE Greenland shelf with a special focus on the interval ca. 870–1910 Common Era (C.E.) reconstructed in subdecadal temporal resolution. The Medieval Climate Anomaly (MCA) between 1000 and 1200 C.E. represents the warmest ocean surface conditions of the SE Greenland shelf over the late Holocene (880 B.C.E. (before the Common Era) to 1910 C.E.). It was characterized by abrupt, decadal to multidecadal changes, such as an abrupt warming of ~2.4°C in 55 years around 1000 C.E. Temperature changes of these magnitudes are rare on the North Atlantic proxy data. Compared to regional air temperature reconstructions, our results indicate a lag of about 50 years in ocean surface warming either due to increased freshwater discharge from the Greenland ice sheet or intensified sea ice export from the Arctic as a response to atmospheric warming at the beginning of the MCA. A cool phase, from 1200–1890 C.E., associated with the Little Ice Age, ends with the rapid warming of aSST and diminished aSIC in the early twentieth century. The results show that the periods of warm aSST and aSIC minima are coupled with solar minima suggesting that solar forcing possibly amplified by atmospheric forcing have been behind the variability of surface conditions on the SE Greenland over the last millennium. The results indicate that the SE Greenland shelf is a climatologically sensitive area where extremely rapid changes are possible and highlights the importance of the area under the present warming conditions.

### 1. Introduction

Both freshwater and sea ice export from the Arctic Ocean by the cold East Greenland Current (EGC) as well as freshwater discharge from the Greenland ice sheet (GIS) affect sea surface temperature (SST) in the North Atlantic. This affects in turn the surface circulation in the North Atlantic subpolar gyre, and the intensity of the North Atlantic Deep Water formation both in the Greenland and Labrador Seas with major implications for the Atlantic Meridional Overturning Circulation (AMOC) and the North Atlantic climate [e.g., *Blaschek et al.*, 2015; *Yu et al.*, 2015].

Despite the potential climatic impacts of changes in freshwater balance from the SE Greenland area, very few geological proxy records of ocean surface conditions covering the last millennium exist from this area. Studies at a low temporal resolution indicate that the Neoglacial interval from ca. 3.0 to 0.2 cal ka B.P. was cold and variable with increased freshwater forcing from the Arctic Ocean [*Andersen et al.*, 2004a, 2004b; *Jennings et al.*, 2011] though characterized by a slow warming trend [*Jennings et al.*, 2011]. *Andersen et al.* [2012] found from cores Fox04G/05R near Sermilik Fjord that the area was dominated by cold low-salinity water masses from 1.5 cal ka B.P., until the subsurface conditions turned warmer at 0.7 cal ka B.P. Lithofacies and benthic foraminiferal analyses from Nansen Fjord, eastern Greenland, suggest that the climate in the area was warmer and more stable than today during the MCA ca. 730–1100 Common Era (C.E.), whereas variable climatic conditions with frequent intervals of severe cold characterize a Little Ice Age (LIA)-type interval ca. 1630–1900 C.E. [*Jennings and Weiner*, 1996]. Only one SST study from the SE Greenland shelf has focused on decadal- to centennial-scale variability of the last millennium. In the diatom-based study on the core MD99-2322 for the time interval 1150–1740 Common Era (C.E.), *Justwan et al.* [2009] did not observe any clear warm or cold phases associated with the known climate anomalies of the last millennium. Farther to the southwest, in the ca. 1500 yearlong record from Igaliku Fjord, SSW Greenland [*Jensen et al.*, 2004], a cold climate regime changed to the warm Medieval Climate Anomaly (MCA) observed between 800 and 1250 C.E. and characterized by cooling events between 960 and 1140 C.E. The MCA was followed by a variable

transitional period, and cold conditions during the Little Ice Age (LIA) prevailed for 1580–1850 C.E. Overall, no clear MCA signal of warm sea surface conditions have not been reported in the SE Greenland shelf area according to previous studies.

The climate of the last millennium featured distinct centennial- to decadal-scale variability with well-documented societal impacts. As future climate changes will be a result of an interaction between the natural and anthropogenic forcing, better understanding of the mechanisms behind recent natural climate anomalies will improve predictions of future variability. The MCA and the LIA are commonly considered to occupy the time periods of ca. 950–1250 C.E. and 1400–1900 C.E. in the North Atlantic region [e.g., Lamb, 1965; Grove, 1988; Mann *et al.*, 2009; Berner *et al.*, 2011; Graham *et al.*, 2011; Goosse *et al.*, 2012]. Many regional aspects of these anomalies require further investigations, such as the timing of the anomalies in the Holocene climatic context, the spatial extent and local expression, associated forcing factors, and their relative magnitudes compared with the modern instrumental temperature records and the twentieth century warming [e.g., Xoplaki *et al.*, 2011].

Although several marine high-resolution SST proxy records have been published from the northern North Atlantic during the last few years [e.g., Berner *et al.*, 2008, 2011; Miettinen *et al.*, 2011, 2012; Ran *et al.*, 2011; Sicre *et al.*, 2011, 2014; Jiang *et al.*, 2015], these records are still too sparse for inferring the decadal- to multidecadal-scale spatial manifestation of the MCA and LIA in the northern North Atlantic realm. The situation is even worse with sea ice proxy data as few quantitative high-resolution records exist [e.g., Justwan and Koç, 2008; Masse *et al.*, 2008; Sha *et al.*, 2014]. Therefore, we have reconstructed August sea surface temperature (aSST) and April sea ice concentration (aSIC) at subdecadal temporal resolution based on diatom assemblages from sediment core MD99-2322 from the Kangerlussuaq Trough, SE Greenland shelf in order to investigate the variability of summer sea surface conditions along with possible forcing factors on the climatologically sensitive SE Greenland shelf during the last 1130 years (Figure 1). While several climate proxies have already been published from the core, e.g., ice-rafted detritus (IRD), biogenic calcium carbonate, benthic and planktonic foraminiferal assemblages and  $\delta^{18}\text{O}$ , planktonic foraminiferal derived summer subsurface temperatures for the Holocene [Jennings *et al.*, 2011; Andrews and Jennings, 2014], and diatom-derived SST reconstruction for interval 1150–1740 C.E. [Justwan *et al.*, 2009], this is the first effort to quantitatively reconstruct surface conditions in the area over the two major climate anomalies of the last millennium with subdecadal-scale time resolution.

## 2. Oceanographic Setting

The studied core site in the Kangerlussuaq Trough is located on the SE Greenland shelf, adjacent to Denmark Strait, and is primarily influenced at the sea surface by the cold East Greenland Current (EGC) (Figure 1). The EGC is an important link between the Arctic Ocean and the North Atlantic Ocean. It is the major southward flowing cold surface ocean current in the Greenland Sea and North Atlantic. It transports Arctic Ocean water masses, recirculating Atlantic Water, and >90% of the ice exported from the Arctic Ocean [Rudels *et al.*, 1999; Woodgate *et al.*, 1999]. The EGC flows southward along the eastern coast of Greenland from Fram Strait to Cape Farewell through the Greenland Sea and the Denmark Strait [Woodgate *et al.*, 1999]. Part of the EGC branches toward the east in the north of Iceland forming the East Iceland Current (EIC). Within the Denmark Strait, the EGC converges with the southwest flowing Irminger Current (IC) forming the marine Polar Front. The IC is the continuation of the western branch of the North Atlantic Current (NAC) and a part of the North Atlantic subpolar gyre. It is composed of warm and saline Atlantic waters from the eastern North Atlantic. These Atlantic waters enter the Kangerlussuaq Trough as Irminger Atlantic Water (IAW), an intermediate layer between the Polar Water and Atlantic Intermediate Water of the EGC [Jennings and Helgadottir, 1994]. The IAW is a distinctly warmer and more saline water mass than the return Atlantic Water of the EGC [Jennings *et al.*, 2011]. South of Greenland, the waters of the EGC and IC are incorporated into the West Greenland Current (WGC) which finally enters the Labrador Sea. Variability in fresh water export with WGC has further implications for the strength of deep water formation in the Greenland and Labrador Seas and thus exerts a general influence on climate through the associated changes in the vigor of the AMOC.

Modern climate conditions at the core site were assessed using NOAA's Extended Reconstruction SST archive for 1854–2014 (ERSSTv3b) [Smith *et al.*, 2008] and the satellite-based SSM/I sea ice concentrations for 1979–2014 [Cavalieri *et al.*, 1996]. Proximity of the oceanographic frontal zone (polar front) associated with large spatial temperature gradient together with the site location on the border of the four grid cells in the

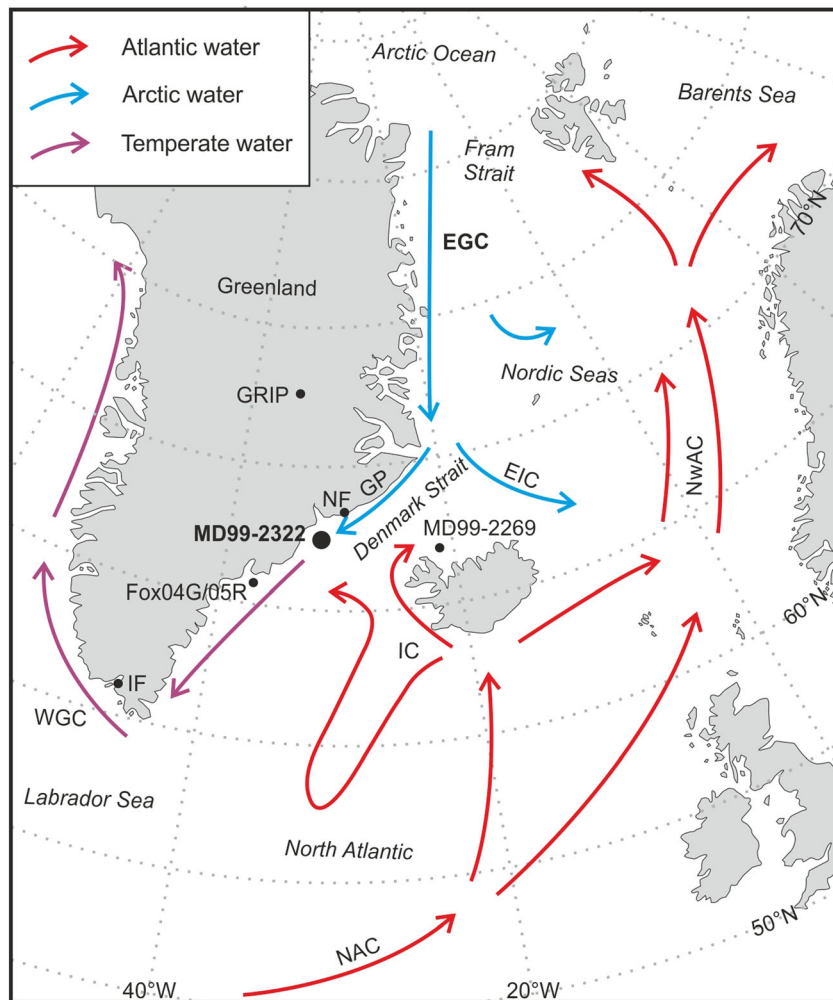


**Figure 1.** Location of the core site MD99-2322 on the SE Greenland shelf and the other sites mentioned in the text. The major surface currents in the North Atlantic and Nordic Seas: East Greenland Current (EGC), East Icelandic Current (EIC), Irminger Current (IC), west Greenland Current (WGC), Norwegian Atlantic Current (NwAC), North Atlantic Current (NAC). IF = Igaliku Fjord, NF = Nansen Fjord.

ERSST domain conditions highly variable estimates of modern August SST over the period of 1854–2009 with a median SST of 5.5(1.7)°C (Figure S1a in the supporting information). A bimodality of the aSST probability density for the area results from insufficient spatial resolution of the ERSST archive. Modern median April sea ice concentration of 84% was for consistency, estimated for the same geographical area of 4° by 4° latitude/longitude as for the aSST. The result is very similar even if only one 25 km pixel of the SSMI grid is used (Figure S1b). Note that in both cases the median values are used instead of sample means to account for the non-Gaussian distributions of the analyzed variables.

### 3. Material and Methods

#### 3.1. Material

Core MD99-2322 was recovered from the SE Greenland shelf (67°08.18'N, 30°49.67'W) from the deepest part of the Kangerlussuaq Trough from a water depth of 714 m during the IMAGES cruise, Leg 4, in 1999 by R/V *Marion Dufresne*. The core was sampled for diatoms in the uppermost 316 cm representing the last ~2900 years. The interval 155–316 cm was subsampled at ca. 4.0 cm intervals. In this work, we primarily focus on the uppermost 155 cm of the core representing the last ~1100 years. This core segment was subsampled continuously at 0.5 cm intervals for the uppermost 20 cm and at 1.0 cm intervals between 20 and 155 cm.

**Table 1.** Accelerator Mass Spectrometer Radiocarbon Measurements, Tephra, and Calibrated Calendar Dates for Core MD99-2232, Including Depth-Correlated Dates From Core MD99-2269

Depth (cm)	Core ID	Radiocarbon Laboratory Number	Material Dated	<sup>14</sup> C Age (year B.P.)	Med. Calibr. Date (year A.D.)	Sigma (years)	Modeled 95% CI (A.D. from)	Modeled 95% CI (A.D. to)
0 (top)	2322				1917	26	1863	1951
34	2322	AA40050	<i>Colus turgidulus</i>	693 ± 38	1649	25	1591	1693
101.5	2322	AA49380	Mixed forams	1267 ± 44	1191	29	1132	1251
154.5	2322			Settlement tephra	870	2	865	874
160	2269	AA47785	<i>Macoma</i> sp.	1693 ± 42	765	29	701	825
187	2269	AA57895	cf. <i>Yoldia glacialis</i>	1978 ± 35	427	37	356	511
227	2269	AA54590	cf. <i>Macoma balthica</i>	2396 ± 47	-30	33	-96	36
232.5	2322	CURL-15479	Mixed benthic forams	2415 ± 20	-85	30	-148	-29
258	2269	AA38586	<i>Yoldia</i> cf. <i>myalis</i>	2578 ± 48	-326	36	-389	-247
310	2269	AA57896	<i>Yoldia</i> sp.	3017 ± 39	-828	33	-898	-772
360	2269	AA54592	Mixed benthic forams	3375 ± 80	-1303	41	-1380	-1219
368	2322	AA49382	bivalve	3451 ± 39	-1380	39	-1451	-1296
415	2269	AA57897b	<i>Arca glacialis</i>	3840 ± 33	-1822	48	-1917	-1732

### 3.2. Chronology

The age model for the topmost section of core MD99-2322 is based on five accelerator mass spectrometry (AMS) <sup>14</sup>C datings on benthic foraminifers and mollusks [see Stoner *et al.*, 2007; Jennings *et al.*, 2011] (Table 1). Due to calcification in Atlantic Water, benthic foraminifera and mollusks are suitable for dating on the SE Greenland shelf as the problems with radiocarbon dating from the deep sea sediments showing very old ages for benthic foraminifera do not appear in this area. The age control was further improved by including seven dates from core MD99-2269 retrieved from the north Iceland shelf. These AMS dates comprise a subset of dates from Stoner *et al.* [2007] used for the construction of the entire 2617 cm long commingled core chronology via synchronization of the respective paleomagnetic secular variation series for the two sediment cores [Stoner *et al.*, 2007]. Note, however, that here the uppermost date C5734 from 2.5 cm core depth was discarded from the analysis as providing unrealistically high sedimentation rate for the most recent 300 years. The age model is supplemented by a tephra layer at 154.5 cm core depth associated with a Vatnaöldur eruption (Settlement tephra) and dated to 871 ± 2 C.E. [Jennings *et al.*, 2014].

We applied the OxCal 4.2 [Bronk Ramsey, 2008, 2009] software for raw AMS dates calibration using the radiocarbon calibration curve IntCal13 [Reimer *et al.*, 2013] and calculation of the age-depth model. A marine reservoir correction of 400 years was assumed for core MD99-2322. The age model provides a good match in age between the known age settlement tephra and the neighboring AMS date. OxCal was initiated with a Poisson process deposition model [Bronk Ramsey, 2008; Bronk Ramsey and Lee, 2013] with *k* parameter of the model set to *k* = 1, to allow for fluctuations in the sedimentation rate at a characteristic scale of 1 cm and the core top age set to U(1850,1950) corresponding to any arbitrary date within the interval of 1850–1950 C.E. The age distributions for points between the dated horizons were also generated with a regular depth interval of 0.5 cm.

Previous studies from a nearby area north of Iceland affected by polar water indicate that reservoir ages of these waters can be even up to 450 years older than the standard model ocean [Eiriksson *et al.*, 2004, 2011]. The dated foraminifera and mollusks of this study have been calcified in well-equilibrated Atlantic Water that originates from the NAC. Since they have not dwelled in the “old” polar water, we did not introduce any additional reservoir correction, i.e., set Δ*R* = 0. We however admit that a higher and variable Δ*R* might have occurred through time also in our data. Since this cannot be inferred explicitly from the available data, a common reservoir correction of 400 years was used consistently in the MD99-2322 age model throughout the entire Holocene section of the core [Jennings *et al.*, 2006; Stoner *et al.*, 2007]. The use of this marine reservoir correction is further supported by three tephra layers: 12,000 year old Vedde Ash, the 10,200 year old early Holocene Saksunarvatn tephra [Grönvold *et al.*, 1995; Jennings *et al.*, 2002], and the Settlement tephra (871 ± 2 C.E.) [Jennings *et al.*, 2014]. We note, however, that the regional variability of Δ*R* is large. For example, a larger Δ*R* was used in the northern Denmark Strait [Jennings *et al.*, 2002, 2006] to account for a stronger influence of Polar Water in the area.

The resulting age model for the core MD99-2322 features a smooth almost linear sedimentation throughout the last 3800 years with an average sedimentation rate for this period of ~0.1 cm yr<sup>-1</sup> (Figure 2).

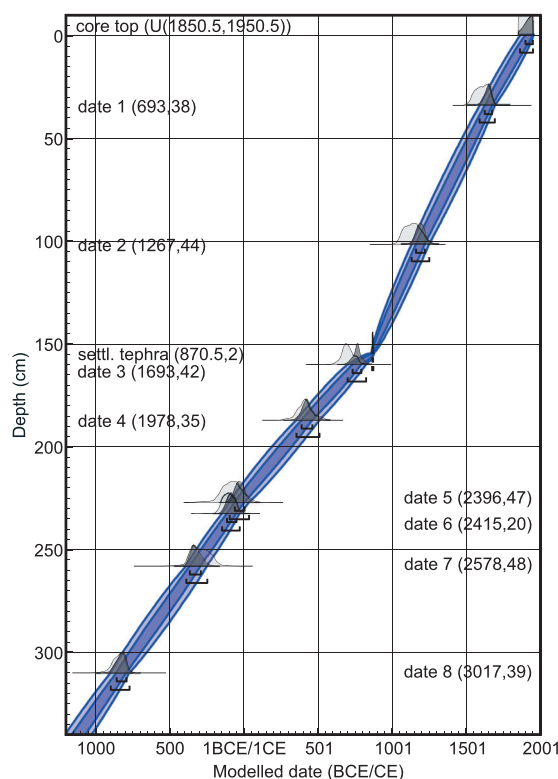


**Figure 2.** The OxCal age model for the topmost section of the core MD99-2232 based on 11 AMS dates and one tephra layer. The reported  $^{14}\text{C}$  ages in years B.P. with the respective  $1\sigma$  uncertainty for the dates used are given in parenthesis. Dark and light blue envelopes outline the 68% and 95% probability density ranges for the depth age model. Light grey shows the probability distributions (likelihoods) for single calibrated dates; their marginal posterior distributions which take into account the constructed depth age model are shown in dark grey.

### 3.3. Diatom Analysis

Planktonic diatoms are good indicators of surface water conditions (e.g., SST, sea ice) in the Nordic Seas [e.g., Koç-Karpuz and Schrader, 1990; Andersen et al., 2004a; Jiang et al., 2005, 2015], because they show good analogue relations to modern oceanic conditions, live in the uppermost surface waters (0–50 m), and are abundant in polar to temperate, nutrient-rich regions. Core MD99-2322 was analyzed for diatoms continuously at a temporal resolution of  $\sim 3$  years for the period of 1750–1910 C.E. according to our age-depth model and at a resolution of 5–8 years for the period of 870–1750 C.E. The period 880 B.C.E. to 870 C.E. was analyzed at the lower resolution of 40 years. In this study, we focus on the high-resolution interval 870–1910 C.E., which enables us to reconstruct the climate changes on the SE Greenland shelf at the highest resolution to date. The diatom samples were prepared using the method described by Koç et al. [1993] consisting of HCl and  $\text{H}_2\text{O}_2$  treatment, clay separation, and preparation of quantitative slides. A Leica Orthoplan microscope with 1000X magnification was used for identification and counting of diatoms. The counting procedure described by Schrader and Gersonde [1978] was followed and  $\geq 300$  diatom frustules (excluding *Chaetoceros* resting spores) were identified from each sample. *Chaetoceros* resting spores were excluded because they show negligible sensitivity to SST, and they can dominate the diatom assemblage biasing the reconstructions [Koç-Karpuz and Schrader, 1990].

#### 3.3.1. Reconstruction of Paleo SST

An extended calibration data set consisting of 184 surface sediment samples from the North Atlantic, the Labrador Sea, the Nordic Seas, and Baffin Bay with 52 diatom species was utilized to convert diatom counts to aSSTs using the weighted averaging partial least squares (WA-PLS) transfer function method [Ter-Braak and Juggins, 1993]. The previous diatom SST calibration data set of Andersen et al. [2004a] including 139 surface samples with 52 diatom species from the North Atlantic and the Nordic Seas has been successfully used in quantitative diatom-based SST reconstructions from the high-latitude oceans [Andersen et al., 2004a, 2004b; Berner et al., 2008, 2010, 2011; Justwan et al., 2009; Miettinen et al., 2011, 2012]. In order to improve its temperature range for colder SST, the data set was extended by 23 new surface sediment samples recovered from the East Greenland and West Spitsbergen margins, Greenland Basin, and Fram Strait during WARMFAST cruises by the R/V *Jan Mayen* in 2006, 2007, and 2008 (Figure S2). In addition, 13 samples were taken from Baffin Bay by the R/V *CCGS Hudson* and 10 samples from the Labrador Sea by R/V *Maria S. Merian* in 2008. The data set provides a good fit for observed aSST in WOA01 data [Stephens et al., 2002] versus reconstructed aSST (Figure S3). Extending the calibration set with samples collected from the areas associated with generally cold (1–6°C) summer SST made it into a tool of high potential for quantitative SST reconstructions also in the Arctic regions. August was chosen as a target month for the reconstruction procedure, because for diatom transfer functions the August SST gives the best match with respect to observed sea surface temperatures [cf. Berner et al., 2008]. The updated WA-PLS diatom transfer function has a root-mean-square error (RMSE) of 0.80°C, a coefficient of determination between observed and inferred values ( $r^2$ ) of 0.96, and a maximum bias of 0.60°C.

### 3.3.2. Reconstruction of Paleo Sea Ice Conditions

A subset of the main calibration set comprising 89 surface sediment samples from the northern North Atlantic, the Nordic Seas, Baffin Bay, and northwestern Labrador Sea was created for a quantitative reconstruction of April sea ice concentrations in the study area. For calibration we used modern satellite-based sea ice concentrations from the sampling locations and the WA-PLS transfer function method. In total, 19 surface sediment samples were selected from the East Greenland and West Spitsbergen margins, Greenland Basin, and Fram Strait, 13 samples from Baffin Bay, and 8 samples from the Labrador Sea (Figure S4). The remaining 49 samples from the Nordic Seas were adopted from the data set published earlier by Andersen *et al.* [2004a]. Some of these samples were also used by Justwan and Koç, [2008] in their sea ice transfer function built using a different modern sea ice training data set (based on surface samples taken prior to 2004 and May sea ice concentration from 1998 as a modern environmental variable) and a different reconstruction technique (maximum likelihood). In our data set, modern monthly sea ice concentrations from 1979 to 2012 were obtained from the National Snow and Ice Data Center (NSIDC, [www.nsidc.com](http://www.nsidc.com)) [Cavalieri *et al.*, 1996]. Compilations of monthly sea ice data were made for interval 1979–1999 for the sites in the data set of Andersen *et al.* [2004a], for intervals of 1979–2006, 1979–2007, and 1979–2008 for the surface samples taken in 2006, 2007, and 2008, respectively. A five-component WA-PLS model was selected for the transfer function. The novel WA-PLS diatom sea ice transfer function has a RMSE of 13.1%,  $r^2$  of 0.86, and a maximum bias of 13.1% with respect to observed sea ice concentrations. The sea ice data set provides a good fit for observed April sea ice data versus reconstructed aSIC (Figure S5).

In addition, the occurrence of two sea-ice-related diatom species *Fragilariopsis cylindrus* and *F. oceanica* (hereafter *Fragilariopsis* spp.) was qualitatively used in order to get more information about sea ice conditions. *Fragilariopsis* spp. are common species in the pack ice and in the water column near the ice edge, especially during Arctic spring blooms, often associated with the onset of melting sea ice [e.g., von Quillfeldt, 2001]. They appear to have the strongest loadings in sea-ice-associated assemblages among diatoms in this region [e.g., Jiang *et al.*, 2001; Ran *et al.*, 2011].

### 3.4. Other Statistical Analysis

The wavelet-transform-based technique was applied for the bandpass filtering and visualization of the quasiperiodic behavior in the analyzed data series [Torrence and Compo, 1998]. We used the Morlet wavelet as a basis function which is believed to be an optimal choice to provide a good balance between time and frequency localization for features in wavelet spectra. Prior to analysis, the data series were resampled using the time interval of 10 years; the gaps in the resampled series were filled using spline interpolation for creating a time scale with a regular time increment.

Wavelet coherence analysis [Grinsted *et al.*, 2004] was also used to examine relationships between the pairs of records on different time scales. The method shows how coherent two wavelet spectra being analyzed are and can be thought of as a localized correlation coefficient in time frequency space.

## 4. Results and Discussion

The low-resolution data for interval 880 B.C.E. to 870 C.E. are briefly presented here in order to put the SST variability of the last millennium to a longer late Holocene context. This interval shows cool conditions and the August sea surface temperature (aSST) range from 4.0 to 6.7°C including the cold period between ~500 B.C.E. and 600 C.E., and warmer periods for intervals ~880–500 B.C.E. and ~600–800 C.E. (Figure 3a). The results for sea ice indicate a pronounced influence of the sea ice for this low-resolution interval with the exception of the short periods ~750–500 B.C.E., ~300 C.E., and 600–900 C.E., respectively.

The aSST reconstruction for the high-resolution interval 870–1910 C.E., shows a total aSST range from 4.5 to 7.2°C (Figure 4) which is in line with the modern estimates for the area (Figure S1). We divide the record into six periods based on the reconstructed temperatures above or below the mean SST of 5.5°C of the record; cold period 870–1000 C.E., warm 1000–1200 C.E., cool 1200–1600 C.E., relatively warm 1600–1820 C.E., cold 1820–1890 C.E., and warm period 1890–1910 C.E. The aSST record shows some abrupt changes and clear centennial-bicentennial variability for this interval which is apparent from the bandpass-filtered series shown in Figure 5.

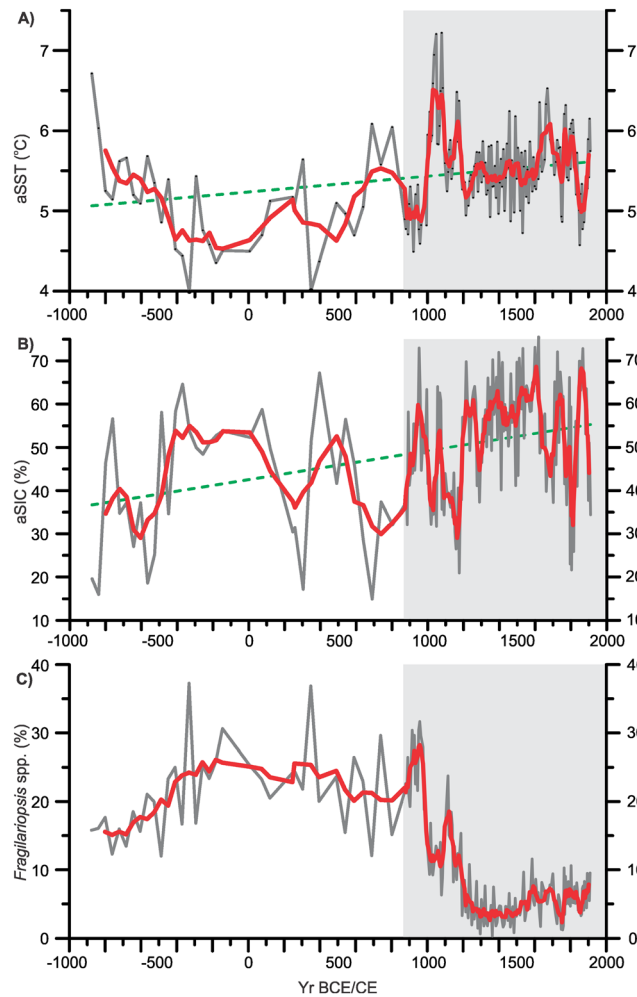


**Figure 3.** Paleoproxy reconstructions for core MD99-2322 for interval 880 BCE–1910 CE. (a) aSST reconstructions, (b) aSIC reconstruction, and (c) *Fragilariopsis* spp. Red lines indicate smoothed records (5 points) and green dotted lines show linear trends. The shaded area shows the interval 870–1910 CE with reconstructions on a subdecadal temporal scale shown on Figure 4.

~55 years, indicating a forceful onset of the warm conditions in the area. The clearly discernible warm period ~1000–1200 C.E. with the mean aSST of 6°C represents the warmest interval of the 2900 year long record (though the existence of decadal-scale warming events during the interval of lower temporal resolution 880 B.C.E. to 870 C.E. cannot be ruled out), and it can be associated with the local expression of the MCA. Climate conditions in the area during the MCA, however, remain unstable featuring pronounced decadal to multidecadal-scale variability. In particular, the warmest aSST phase of the MCA is punctuated by a 10 year long cooling episode with high aSIC ~1060 CE. The latter temperature peak is again (~1100 C.E.) followed by a cooling of a similar magnitude (~2°C) as the warming some 100 years earlier. The prominent warm double SST peak is the most significant feature in this aSST record. Temperature changes of this magnitude are rare in the North Atlantic proxy data, though a pronounced temperature maximum was also detected in the lower resolution subsurface temperature record from this site at ~0.8 cal ka B.P. [Jennings et al., 2011]. After the double aSST peak around 1100 C.E., despite the aSST cooling, the aSIC decreases to the lowest level of the last millennium for the interval 1100–1200 C.E., still *Fragilariopsis* spp. shows again a higher level. This cooling does not yet indicate the local termination of the MCA as after this short ca. 50 year long cooler phase, a second warm aSST peak (aSSTs ~6.5°C) follows between 1150 and 1190 C.E. simultaneously with the aSIC minimum of the MCA. Until finally, an abrupt cooling of 1.5°C over 40 years marks the termination of the

For the last millennium, the results for sea ice first indicate persistently high aSIC for the long interval between 1200 and 1600 C.E., followed by shorter multidecadal to centennial periods of variable sea ice conditions until 1910 C.E. (Figure 4). A strong influence of sea ice in the area is in line with the modern situation as today: Kangerlussuaq Trough sea ice covered some 6.5–9.5 months a year [Jennings et al., 2011, see also Figure S1b]. Sea-ice-related diatom species (*Fragilariopsis* spp.) show higher proportions for the interval 870–1200 C.E. (especially 870–980 C.E. > 20%) while they remain at a relatively low level (<10%) in the subsequent period until the very top of the record.

#### 4.1. The Medieval Climate Anomaly

A cold period between 870 and 1000 C.E. represents the coldest interval of the high-resolution reconstruction over the considered time interval (Figure 4). The average aSST of the period is ~5°C and the coldest aSST observation (4.5°C) of the record is dated to ~920 C.E. The diatoms indicate a high sea ice concentration for this period; both aSIC and specific sea ice indicators (*Fragilariopsis* spp.) show high levels reaching their maximum ~980 C.E., after which they start to decline rapidly.

Around 1000 C.E., aSST rises as much as ~2.4°C from 4.8°C (~995 C.E.) to the absolute record maximum of 7.2°C (~1050 C.E.) in the time span of only

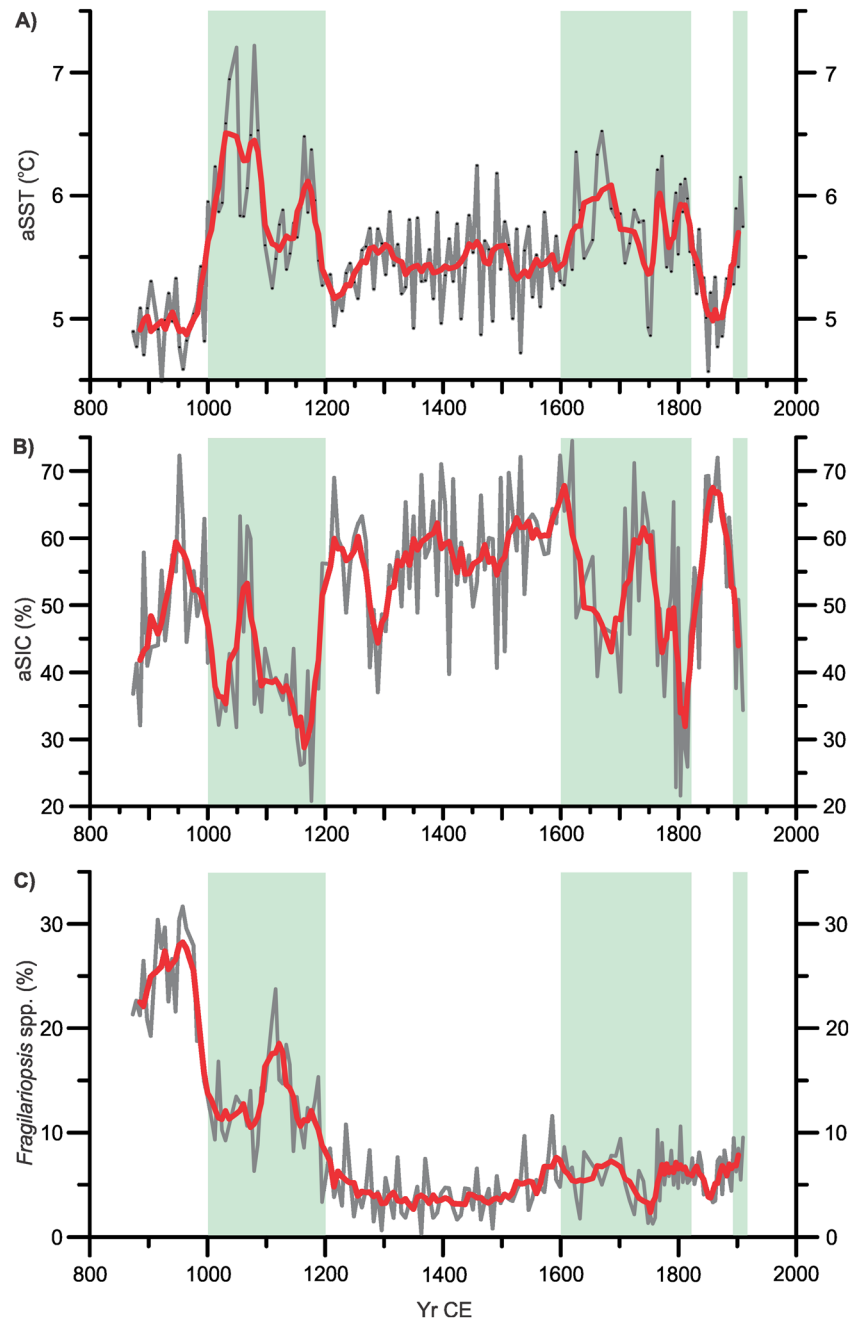


**Figure 4.** High-resolution paleoceanographic reconstructions for core MD99-2322 for the interval 870–1910 CE. (a) aSST reconstruction, (b) aSIC reconstruction, and (c) *Fragilariopsis* spp. Red lines indicate smoothed records (5 points). Shaded areas show warm periods inferred from the aSST record.

warm MCA around 1200 C.E. At the same time, the aSIC rises rapidly to a high level. *Fragilariopsis* spp. do not follow the robust rise of the aSIC. Instead, they show a rapid decline in parallel with the termination of the warm period and remain at a considerably lower level than was seen during the MCA until the end of record.

Based on the Northern Hemisphere spatial surface air temperature (SAT) reconstruction, *Mann et al.* [2009] identify the MCA as a 300 year long interval from 950 to 1250 C.E. with the warmest phase between 950 and 1100 C.E. In the Arctic SAT reconstruction [*Kaufman et al.*, 2009], the MCA spans the same interval as the Northern Hemisphere SAT 950–1250, but the highest Arctic temperatures are reconstructed for the

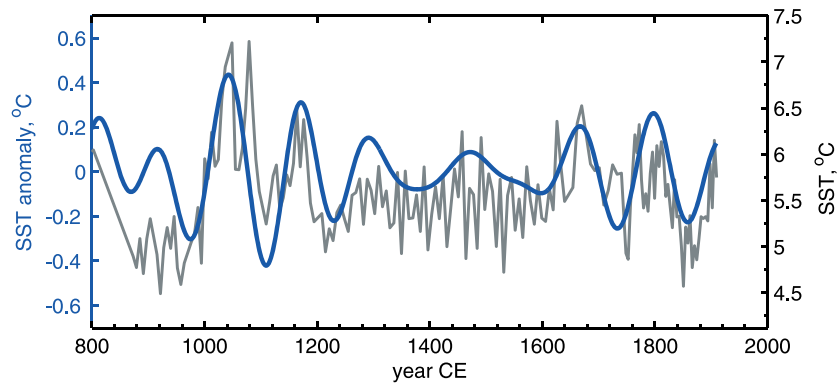


**Figure 5.** The aSST reconstruction (grey) and the bandpassed aSST variability in the bandwidths of 100–250 years (blue) for core MD99-2322.

relatively short interval 920–980 C.E. (Figure 6). More locally, the summer Greenland Ice Core Project (GRIP)  $^{18}\text{O}$  data [Vinther *et al.*, 2010], shows high values around 950 C.E. indicating warmer temperatures for this time interval in Greenland (Figure 6). Generally, the observed ~200 year long warm oceanic MCA on the SE Greenland shelf between 1000 and 1200 C.E. agrees well with the spatial SAT reconstruction by Mann *et al.* [2009] (not shown). In contrast, the reconstructed MD99-2322 aSSTs were still cold with severe sea ice conditions including the highest percentages of *Fragilariopsis* spp. at the beginning of the warmest stage of the SAT anomaly during 950–1000 C.E. The observed lag of about 50 years in the reconstructed aSST relative to SATs and Greenland ice core data indicate a delayed onset of ocean surface warming on the SE Greenland shelf at the beginning of the MCA in 950–1000 C.E. The end of the prominent SST peak on the SE Greenland shelf is synchronous with a subtle cooling in SAT reconstructions around 1100 C.E. However, again the onset of termination of the warm marine stage on the SE Greenland shelf around 1200 C.E. leads by ~50 years the termination of the MCA in the Northern Hemisphere and the Arctic demonstrated in previous studies [e.g., Jensen *et al.*, 2004; Kaufman *et al.*, 2009; Mann *et al.*, 2009].

Interestingly, the summer GRIP  $^{18}\text{O}$  maxima of the MCA occurred at ~950 and ~1200 C.E. corresponding to the cold phases in the ocean surface conditions on the SE Greenland shelf. One can hypothesize that high temperatures in Greenland presumably led to an intensified melting of the GIS and thus an increased fresh water flux to the ocean on the eastern Greenland coast. On the SE Greenland shelf, sea ice can form both locally and be transported by the EGC from the north. Our results might suggest that the increased fresh water flux from Greenland caused a gradual freshening of the surface waters of the EGC in the Denmark Strait, promoting the formation of sea ice and further cooling of the surface water especially in the early MCA ~950–1000 C.E. This view is supported by a high occurrence of *Fragilariopsis* spp. at this interval as they are usually associated with onset of melting sea ice [e.g., von Quillfeldt, 2001]. The increased concentration of these diatom species can be due to both more intense seeding from melting sea ice in the more intense sea ice export conditions, and/or prolonged and intensified pelagic blooms. Also, the latter is associated with the sea ice as the blooms of these species occur in the area of seasonal ice zone. As *Fragilariopsis* spp. can be associated with melting sea ice, we hypothesize that sea ice with high *Fragilariopsis* abundance might indicate a higher fraction of the first-year ice in the area, which tended to melt faster in warm climate conditions.

Analysis of cores Fox 04G/05R recovered from the area close to the Sermilik Fjord [Andresen *et al.*, 2012] to the southwest of the MD99-2322 core site (see Figure 1) revealed that the interval of 1.5–0.7 cal. ka B.P. covering the MCA was dominated by low-salinity water masses characterized by sea ice, which was formed locally or transported by the EGC. They suggest that an extensive surface melting of Greenland glaciers during the MCA produced large amounts of fresh water significantly adding to the polar water component of the EGC and simultaneously favoring the formation of sea ice in the coastal area. A comparable development was observed in Igaliku Fjord, SSW Greenland, where the warm MCA prevailed for interval 800–1250 C.E., but was punctuated by cooling episodes between 960 and 1140 C.E. [Jensen *et al.*, 2004].

We speculate that the extremely rapid change to warm conditions ~1050 C.E. might represent the crossing of a critical climatic threshold, triggered by a change of some internal or external forcing factor. In this event, as

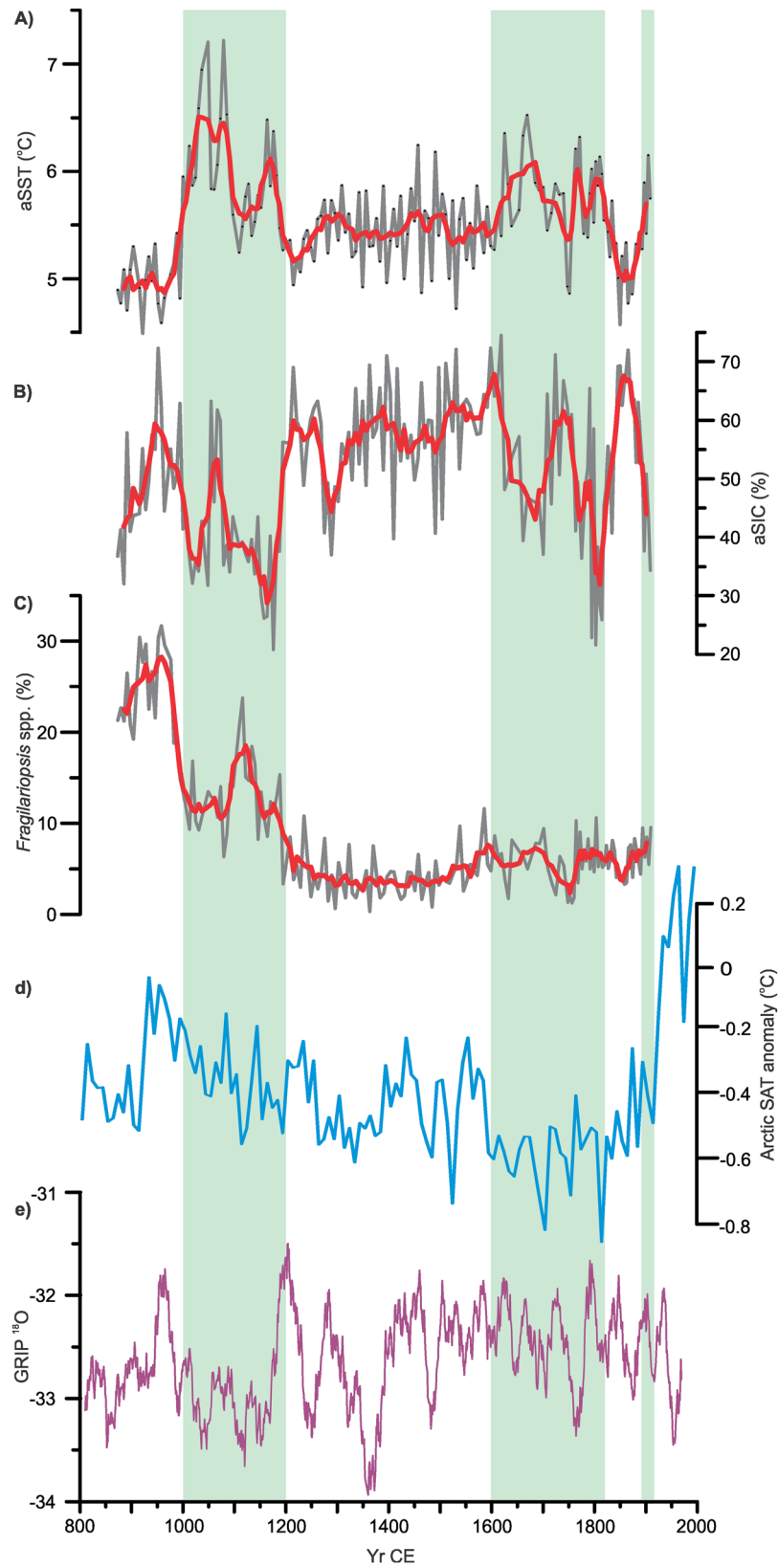


**Figure 6.** (a) aSST for interval 870–1910 CE from the SE Greenland shelf, (b) April sea ice concentration, (c) *Fragilariopsis* spp., (d) Arctic SAT anomaly [Kaufman et al., 2009], and (e) Summer GRIP  $^{18}O$  [Vinther et al., 2010]. Warm aSST periods are shaded.

the amount of melting sea ice decreased on the SE Greenland shelf after the most prominent SAT peak around 1000 C.E., the oceanic factor (i.e., the warmer EGC) was finally able to overcome the sea ice influence and initiated a rapid warming of surface water.

Historically, the MCA represents the well-known period of human expansion in the North Atlantic sector; Norse colonized the North Atlantic islands and eastern North America from 800 to 1000 C.E., Iceland was settled ~874 C.E., and Greenland ~985 C.E. [Arneborg, 2000]. Interestingly, the Norse settled areas in the Southern and Western Greenland but not areas in the SE Greenland though it is located closer to Iceland. We speculate that this has been due to the sea ice conditions in the area. A pronounced variation in sea ice conditions inferred from MD99-2322 during the onset and termination of MCA agrees well with historical evidence from Iceland, specifically a timing of maxima/minima of annual temperatures estimated from the occurrence of drift ice in the area [Bergthorsson, 1969]. A few centuries later, around 1350–1400 C.E., the Norse left southern Greenland [Pringle, 1997]. According to Kuijpers *et al.* [2014], this was due to the colder climate and increased sea ice in the Southern and Western Greenland since ~1200 C.E. Hence, our results on the transition to the cooler conditions on the SE Greenland shelf correspond well with the depopulation of Greenland.

#### 4.2. The Little Ice Age

A shift to persistently colder conditions ~1200 C.E. when aSST dropped rapidly almost to the temperature level that prevailed before the MCA signifies a transition to the cold LIA on the SE Greenland shelf. For the period 1200–1600 C.E., aSST points to cool (the mean aSST ~5.4°C) and variable conditions with decadal-scale variability of relatively high magnitude associated with the LIA. The interval 1200–1260 C.E. initiating the LIA is the second coldest one (with a mean of 5.2°C) over the entire cool climate anomaly indicating a substantial change in ocean surface conditions on the SE Greenland shelf at the transition stage to the LIA. However, aSSTs do not generally decrease to the level that prevailed prior to the MCA. The cool period 1200–1600 is punctuated by two short-term warm phases around 1300 C.E. and ~1440–1510 C.E. After the end of the first warm phase ~1300 C.E., the record shows (sub)decadal variability until 1600 C.E. The second warmer phase (maximum aSST > 6°C) between ~1440 and 1510 C.E. features a pronounced (sub)decadal aSST variability with magnitude exceeding 1°C. At the same time the aSIC indicates a relatively high (sub)decadal variability and increasing sea ice conditions toward the end of the cool period ~1600 C.E. excluding the warmer periods shown by aSST (e.g., ~1300 C.E.). A relatively high climate variability at the shorter time scales in the first part of the LIA was also recorded in the historical Icelandic sources via a more frequent occurrence of both severe and mild seasons in the area [Ogilvie *et al.*, 2000], although a consistency of this relationship throughout the whole period is not apparent.

The time interval of 1600–1820 C.E. was relatively warm with aSST being at the same level as the latter half of the MCA with several superimposed peaks on the decadal to multidecadal time scale. The period is characterized by a high-temperature variability as aSST varies between 4.9°C (~1750 C.E.) and 6.5°C (1670 C.E.). The aSIC shows that sea ice conditions were less severe during this period, except for a short period between 1700 and 1750 C.E. Although also this interval is commonly associated with the LIA between 1400 and 1900 C.E. [e.g., Grove, 1988; Kaufman *et al.*, 2009], several studies indicate warmer conditions for this interval, e.g., warmer spell 1700–1800 C.E. [Mann *et al.*, 2009; Zorita *et al.*, 2010]. However, this warm phase on the SE Greenland shelf does not indicate the lasting shift to the warm conditions as the following interval from 1820–1890 C.E. was the second coldest of the last millennium with the mean 5.2°C. The coldest aSSTs of the LIA prevailed at the end of this cold anomaly, between 1840 and 1880 C.E. with the coldest aSST value (~4.6°C ~1850 C.E.) since 920 C.E. Also, the aSIC attains its highest levels throughout the late Holocene record ~1850 C.E. The record ends on rapidly rising aSST and diminishing of sea ice that can be associated with a recovery from the LIA and the onset of contemporary warming that commenced in the beginning of the twentieth century. During this Warm period ~1890–1910 C.E., the aSST reaches 6.2°C, with an average of 5.8°C for the period.

From the historical perspective, relatively mild sea ice conditions during the extended periods in the 1600s and 1700s are much in line with a lack of sea ice observations around Iceland as was recorded in various written accounts of that period [Ogilvie, 1996]. A sea ice maximum during interval 1850–1890 C.E. followed by a strongly diminished sea ice is in agreement with Divine and Dick [2006] and Alonso-García *et al.*, [2013], who suggest predominantly perennial sea ice conditions for the SE Greenland shelf between

1850 and 1910 C.E., followed by more open water conditions. The high sea ice period is a manifestation of the salinity anomaly (GSA) of the early twentieth century, because there was a clearly registered increased fresh water export from the Arctic at this time [Divine and Dick, 2006]. Its magnitude was similar to (if not higher than) the GSA of the 1960s and the 1970s [Belkin et al., 1998]. The origin of these GSAs has been thought to be the increased outflow of sea ice and freshwater from the Arctic that propagate downstream through the anticlockwise circulation system around the North Atlantic [Dickson et al., 1988; Belkin, 2004].

### 4.3. Forcing Factors Behind the Surface Conditions on the SE Greenland Shelf Over the Last Millennium

The climatological conditions on the SE Greenland shelf are driven by a large number of factors, such as the strength and temperature of the EGC and IC, sea ice formation, fresh water input via iceberg calving, discharge from the Greenland ice sheet, sea ice export from the Arctic, and variable atmospheric and external forcing making the area challenging for paleoceanographic studies [e.g., Alonso-García et al., 2013]. Here we assess the possible contribution/influence of the different factors on the reconstructed surface condition in the study area.

#### 4.3.1. Atmospheric Forcing

Several proxy records indicate that globally the MCA was characterized by coherent shifts in large-scale Northern Hemisphere atmospheric circulation patterns [e.g., Graham et al., 2011]. The positive phase of the Arctic Oscillation (AO)/North Atlantic Oscillation (NAO) has been proposed to play a strong role in the observed changes during the MCA [Shindell et al., 2001, 2003; Seidenkrantz et al., 2007; Mann et al., 2009; Trouet et al., 2009; Sicre et al., 2014]. Goosse et al. [2012] found significant changes in the oceanic near-surface circulation between the MCA and the LIA, e.g., a clear intensification and the northward shift of the subpolar gyre and the Gulf Stream system occurred during the MCA. They also suggested that only a weak forcing was needed to trigger the shift from the MCA to the LIA, with changes in the AMOC playing a relatively minor role in the transition between these two climate anomalies.

Over the last millennium, it is believed that the NAO system has been variable, with a strongly positive NAO mode during the MCA and a neutral to slightly negative mode during the LIA [Trouet et al., 2009]. The positive mode is associated with the increased sea ice export in the East Greenland Current through Fram Strait [e.g., Dickson et al., 2000; Wanner et al., 2001; Olsen et al., 2012; Andrews and Jennings, 2014; Sicre et al., 2014]. The atmospheric forcing might at least partly explain the observed combination of the aSST and the aSIC on the SE Greenland shelf, as under the influence of northerly winds, the cold polar waters and sea ice advance southward freshening the surface water layer, increasing its stratification, and favoring the local sea ice formation [Justwan et al., 2009]. As the increased sea ice export by the +NAO is usually associated with stronger northerly winds and cooling of the surface waters in the Greenland Sea, it is remarkable that the warm aSST period of 1000–1200 C.E. on the SE Greenland shelf partly coincides with the positive NAO mode. However, it is noteworthy that the double-peaked aSST event ends ~1090, i.e., at the same time when the NAO reaches the high positive phase. Thus, the NAO might be behind the cooling of surface waters on the SE Greenland shelf after 1100 C.E.

#### 4.3.2. Ocean Circulation

The range of aSST variability between the aSST maxima of the MCA and the coldest aSST registered during the LIA is considerably high, ~2.7°C. Yet the corresponding difference between the longer-term averages for the two periods is relatively low, ~0.5°C, indicating a relatively mild summer climate during the LIA in the area. The latter can be clearly seen in a longer ~2900 year long context; the LIA cannot be qualified as an exceptionally cold period on the SE Greenland shelf. The ~1100 year long period (500 B.C.E. to 600 C.E.) preceding the MCA was considerably colder than the LIA in the area (Figure 3). This might indicate the influence of the warm Irminger waters on the SE Greenland shelf during the LIA or some other regional factor behind the aSST variability. According to Miettinen et al. [2012], the Irminger waters in the south of Iceland were relatively warm during the LIA due to the intensified subpolar gyre. Also, Andresen et al. [2012] suggest that the warm LIA conditions farther southwest on the SE Greenland shelf were caused by the intensified IC, most likely related to the subpolar gyre variability. A hypothesis of abrupt intensification of the SPG at the MCA/LIA transition in response to intensified volcanic forcing was recently supported by modeling results of Schleussner et al. [2015].

#### 4.3.3. Linkages of the Sea Ice Export and Formation and Fresh Water Discharge

For the last millennium, the results for sea ice indicate the highest reconstructed aSIC for the LIA, i.e., for the long interval between 1200 and 1600 C.E. and for shorter multidecadal periods around 1750 and 1850 C.E. This high-LIA sea ice concentration is a dominant feature also in the longer 2900 year long context. This is surprising in the context of a generally higher aSST during the LIA than the time prior to MCA. This inconsistency might be linked to a different source or/and mechanism for the sea ice formation in the area during the LIA and the time before that anomaly. A high aSIC might be due to the combination of the subpolar gyre variability (which was supposed to be behind the warm aSST) and the intensified EGC polar water transport during the LIA as suggested by *Andresen et al.* [2012]. Near the Greenland coast, this combination would result in stronger stratification favoring sea ice formation as opposed to previous colder aSST periods.

Large variations in the polar planktonic foraminifera *Neogloboquadrina pachyderma* sinistral  $\delta^{18}\text{O}$  in core MD99-2322 after 6 cal ka B.P. suggest inconsistent temperature and salinity conditions at the pycnocline [Jennings et al., 2011]. This may reflect a local freshening of the upper water column by the mixing of IAW with Polar Water in the Kangerlussuaq Trough or with an overall increase in Polar Water as  $\delta^{18}\text{O}$  values of benthic foraminifera show cooling trend for this interval, indicating a progressively increased water column stratification through the Neoglacial interval.

Sea ice diatom species *Fragilariopsis* spp. show higher abundance for the interval 880 B.C.E. to 1200 C.E., i.e., before and during the MCA, whereas its abundance dramatically decreases with the onset of the LIA and never recovers. This observation might indicate a higher fraction of first-year ice (with faster melting rate) during the MCA, whereas the very low abundance of *Fragilariopsis* spp. during the LIA indicates a clearly lower melting rate associated with preferentially thicker multiyear sea ice. This hypothesis is supported by IRD data from the core [Andrews and Jennings, 2014]. The quartz wt % reaches its maximum ~1200 C.E. and has a distinct low during the LIA. This may indicate that the IRD export of sediment from the quartz-rich areas of East Greenland (Figure 1) was restricted either by pervasive landfast sea ice [Reeh et al., 2001; Andrews and Jennings, 2014] or that the increased sea ice in the EGC originated from the Arctic Ocean during the LIA [Andresen et al., 2012].

The proposed hypothesis linking GIS, aSIC, and aSST in the area might be appropriate also for the 1200 year long interval preceding the MCA showing cool aSST and fairly severe aSIC conditions for the interval between 500 B.C.E. and 600 C.E. although temperatures were relatively high in Greenland at this time [Kobashi et al., 2011]. High and intense local ice production was behind the cool surface conditions on the SE Greenland shelf also at this time. This could explain the late Holocene warming trend on the SE Greenland shelf which is an opposite pattern compared with the regular cooling trend of the Atlantic SST pattern that started at the termination of the Holocene thermal optimum around 6000 years ago [e.g., Andersen et al., 2004a].

We cannot rule out the possibility that the warming of the area is due to the overall warming of the northern subpolar Atlantic [Berner et al., 2008; Miettinen et al., 2012; Schleussner et al., 2015] associated with long-term late Holocene changes of the subpolar gyre extent and strength. Yet with the data available at hand, assessment of the relative roles of the freshwater flux from the north and the Irminger waters in the variability of surface conditions on the SE Greenland shelf at different time scales remains difficult.

#### 4.3.4. External Forcing

Both solar variability and volcanism have been considered the primary external forcing factors behind the LIA cooling [e.g., Crowley, 2000; Shindell et al., 2003; Jiang et al., 2005, 2015; Miller et al., 2012; Schleussner et al., 2015] though their relative roles are still under discussion [e.g., Hegerl et al., 2003; Otterå et al., 2010; Moffa-Sánchez et al., 2014]. Shindell et al. [2003] suggest that the global mean LIA signal can be attributed to both volcanic and solar forcing, but while volcanic forcing may have played a major role in global-scale cooling, the much larger regional changes and probable changes in the frequency of extreme cold events were likely driven primarily by solar variability. Hegerl et al. [2003] indicate that volcanism is substantially more important explaining 40% of the decadal-scale variability during the LIA. However, our aSST data do not demonstrate any apparent agreement with known volcanic eruptions.

The aSST and the aSIC reconstructions for core MD99-2322 have been compared to total solar irradiance (TSI) [Steinhilber et al., 2012] and to the known solar maximum and minima of the last millennium; the Oort minimum (1010–1050 C.E.), the Medieval solar maximum (1075–1240 C.E.), the Wolf minimum (1280–1350 C.E.), the Spörer minimum (1460–1550 C.E.), the Maunder minimum (1645–1715 C.E.), and the Dalton minimum (1790–1820 C.E.) [Eddy, 1978; Schröder, 2005] (Figure 7).

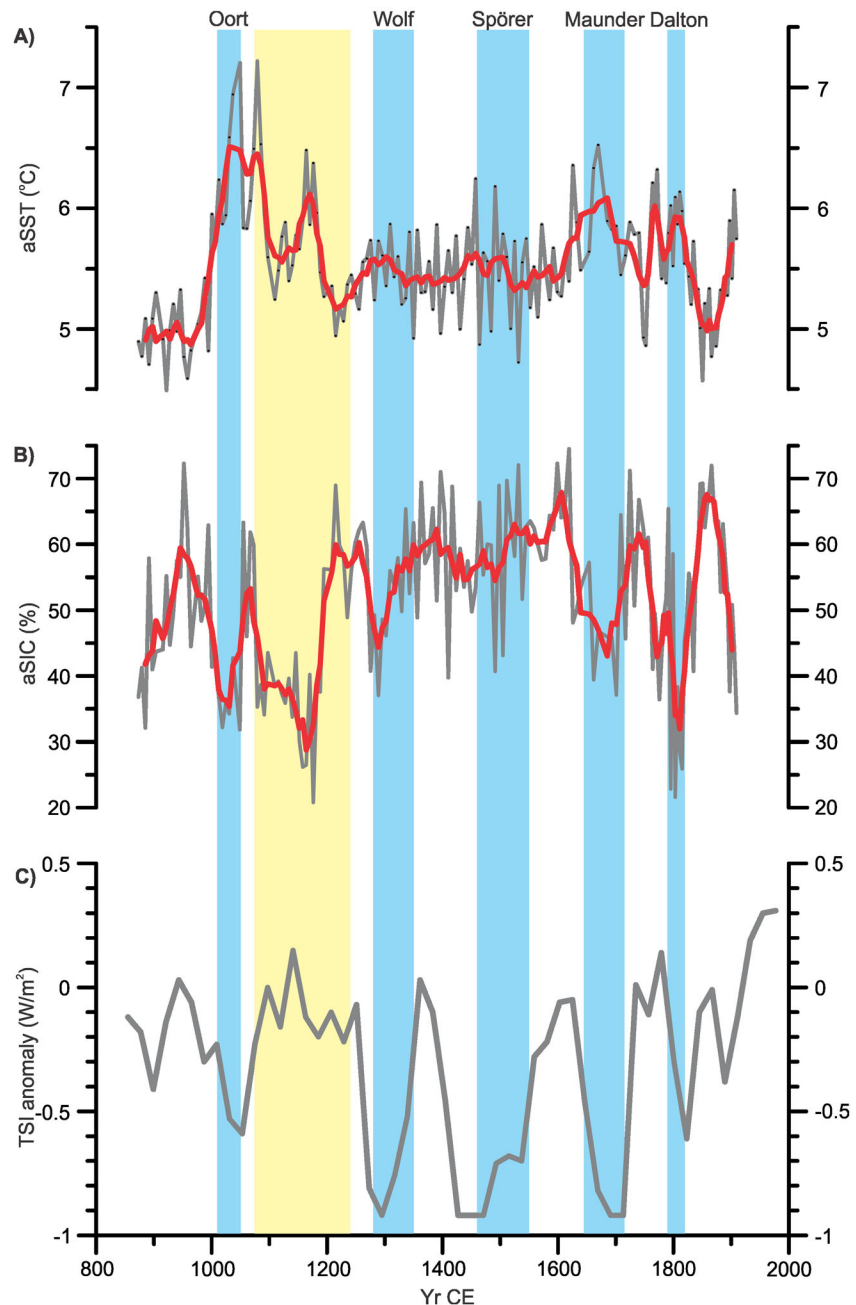


**Figure 7.** The reconstructions of (a) aSST and (b) aSIC for the interval 880–1910 CE, and (c) TSI anomalies and the known solar maximum (shaded yellow) and minima (shaded blue) of the last millennium.

Our ocean surface data agree with the known solar minima, yet this correlation is the opposite to what might be expected from a direct insolation to temperature causal link. For example, the positive correlation between sea ice minima and TSI maxima has been observed in the previous sea ice reconstructions from west of Greenland and the Northern Iceland shelf [Sha et al., 2014]. Our data suggest that most of the warmest multidecadal periods of the aSST record actually match the solar minima. This antiphased relationship is even more clearly visible in the aSIC data, where the wavelet coherence results show a positive coherence between aSIC and TSI in the relatively narrow centennial to bicentennial band of 100–250 years (Figure 8). This suggests that the observed centennial-bicentennial variability of the ocean surface records is at least partly driven by solar forcing.

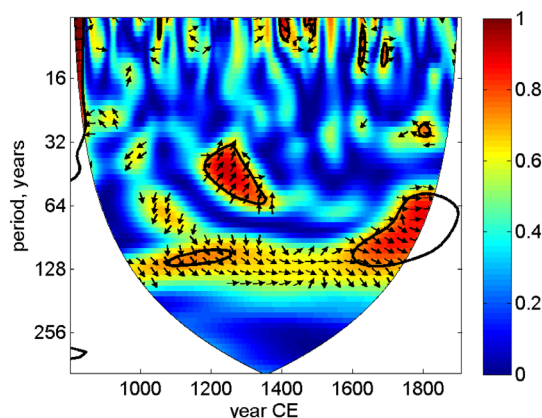


**Figure 8.** Squared wavelet coherence [Grinsted et al., 2004] between the annually interpolated MD99-2322 aSIC and TSI series. Since the wavelet decomposition requires that the data are evenly sampled, the aSIC series was spline interpolated to the annual time scale prior to analysis. Thick contours enclose the areas with correlations statistically significant at 95% confidence level against red noise. The AR1 autocorrelation coefficients of 0.51 and 0.8 of the aSIC and TSI series were estimated from the original data using RedFit [Schulz and Mudelsee, 2002] technique that can analyze the unevenly spaced time series directly. White areas shade the “cone of influence” where the edge effects become important and the results should be interpreted with caution. The relative phase relationship is shown as arrows, with in-phase pointing right and antiphase pointing left.

One might speculate that the solar forcing even triggered the substantial warming of the topmost aSST on the SE Greenland shelf around 1050 C.E., during the MCA. However, it was not the medieval solar maximum behind the initial aSST warming, because the warming started already ~1000 C.E., i.e., some ~80 years before the solar maximum, already during the Oort solar minimum. Thus, it might be possible that it was actually the Oort minimum which locally triggered the rapid warming by decreasing the melting rate of the GIS which further decreased the sea ice formation in our research area. We want to note here that the age control of our data for the early MCA is very accurate due to the identified volcanic tephra marker. Also, during the medieval solar maximum, aSST shows a generally cooling trend until the end of this solar period, though we hypothesize that this cooling is primarily due to the NAO forcing as previously mentioned. However, the long-lasting solar maximum probably also had a warming effect on the surface conditions in the area shown by a minimum aSIC between 1100 and 1200 and simultaneous *Fragilariopsis* spp. peak indicating a higher melting rate for this period. Hence, our results might suggest that over the last millennium, solar forcing, possibly amplified by atmospheric forcing, has been behind the variability of the surface conditions on the SE Greenland shelf.

## 5. Conclusions

The aSST and the aSIC records from the SE Greenland shelf for the last millennium show two major climate anomalies, including abrupt changes and clear centennial-bicentennial variability. The clear warming associated with the local expression of MCA is in an abrupt ~2.4°C warming between 1000 and 1050 C.E., whereas the rapid cooling ~1200 C.E. indicated the transition to the colder LIA conditions. We note that temperature changes of these magnitudes are rare in the North Atlantic proxy data over the last millennium. The reconstructed MCA August sea surface temperatures (up to 7.2°C) represent the highest values reconstructed on the SE Greenland shelf over the late Holocene, between ~870 B.C.E. and 1910 C.E.

The cold ocean surface conditions that prevailed on the SE Greenland shelf during 870–1000 C.E. concurrent with the highest reconstructed air temperatures of the early MCA [Mann et al., 2009; Kaufman et al., 2009] suggest a delayed onset of ocean surface warming on the SE Greenland shelf. This was either due to the influence of the GIS or intensified sea ice export from the Arctic as a response to the atmospheric warming at the beginning of the MCA.

For the interval 1200–1600 C.E., the reconstructed aSST values point to cool and variable conditions with decadal-scale variability of relatively high magnitude associated with the LIA. The period of 1600–1820 C.E. was relatively warm, but it was followed by the coldest interval of the last millennium extending the timing of the LIA on the SE Greenland shelf until ca. 1890 C.E. The difference in the mean values of aSST between MCA and the LIA is, however, only ~0.5°C indicative of relatively mild climate for the LIA due to the influence of warm Irminger waters or different regimes of the sea ice formation during this climate anomaly. The aSST record ends with the rapid warming of aSST in the early twentieth century.

The results show that the phases of warm aSST and aSIC minima on the SE Greenland shelf and the solar minima of the last millennium are antiphased, suggesting that solar forcing possibly amplified by

atmospheric forcing has been behind the aSST variability on the SE Greenland over the last millennium. The results might indicate decreased sea ice formation on the SE Greenland shelf due to diminished freshwater input from the GIS during the cold climate periods.

The composition of surface water is climatically an important factor because the exchange of heat between the ocean and atmosphere takes place on the ocean surface. The results show that the SE Greenland shelf is a climatologically sensitive area where extremely rapid changes are possible. The regional influence of the Greenland ice sheet can be prominent in specific conditions, as seen during the early MCA. Because these oceanic changes can have a global impact through their potential influence on the AMOC, this highlights the importance of Greenland ice sheet and the neighboring ocean with its major surface current, the East Greenland Current, under the present warming conditions.

#### Acknowledgments

We want to acknowledge Olga Pavlova from the Norwegian Polar Institute for collecting the data for the modern sea ice concentrations used in the sea ice transfer function. This paper is a contribution to the International Polar Year (IPY) project “Arctic Natural Climate and Environmental Changes and Human Adaption: From Science to Public Awareness” (SciencePub) funded by the Research Council of Norway, the University of Tromsø, and the Norwegian Polar Institute. The work was partly financed by the Kone Foundation. Thank you to Marit-Solveig Seidenkrantz and an anonymous reviewer for their useful suggestions to improve the manuscript. The reconstructed aSST and aSIC data are available through the databank of NOAA (<http://www.ncdc.noaa.gov/paleo/>).

#### References

- Alonso-García, M., J. T. Andrews, S. T. Belt, P. Cabedo-Sanz, D. Darby, and J. Jaeger (2013), A comparison between multiproxy and historical data (AD 1990–1840) of drift ice conditions on the East Greenland Shelf (~66°N), *Holocene*, *23*, 1672–1683.
- Andersen, C., N. Koç, A. Jennings, and J. T. Andrews (2004a), Nonuniform response to the major surface currents in the Nordic Seas to insolation forcing: Implications for the Holocene climate variability, *Paleoceanography*, *19*, PA2003, doi:10.1029/2002PA000873.
- Andersen, C., N. Koç, and M. Moros (2004b), A highly unstable Holocene climate in the subpolar North Atlantic: Evidence from diatoms, *Quat. Sci. Rev.*, *23*, 2155–2166.
- Andresen, C. S., M. J. Hansen, M.-S. Seidenkrantz, A. E. Jennings, M. D. Knudsen, N. Nørgaard-Pedersen, N. K. Larsen, A. Kuijpers, and C. Pearce (2012), Mid- to late-Holocene oceanographic variability of the Southeast Greenland shelf, *Holocene*, *23*, 167–178.
- Andrews, J. T., and A. E. Jennings (2014), Multidecadal to millennial marine climate oscillations across the Denmark Strait (~66°N) over the last 2000 cal yr BP, *Clim. Past*, *10*, 325–343.
- Arneborg, J. (2000), Greenland and Europe, in *Vikings: The North Atlantic Saga*, edited by W. F. Fitzhugh and E. Ward, pp. 304–317, Smithsonian Inst. Press, London.
- Belkin, I. M. (2004), Propagation of the “Great Salinity Anomaly” of the 1990s around the North Atlantic, *Geophys. Res. Lett.*, *31*, L08306, doi:10.1029/2003GL019334.
- Belkin, I. M., S. Levitus, J. Antonov, S.-A. Malmberg, and A. J. Lee (1998), “Great Salinity Anomalies” in the North Atlantic, *Prog. Oceanogr.*, *41*, 1–68.
- Berghorsson, P. (1969), An estimate of drift ice and temperature in Iceland in 1000 years, *Jokull*, *19*, 94–101.
- Berner, K. S., N. Koç, D. Divine, F. Godtliobsen, and M. Moros (2008), A decadal-scale Holocene sea surface temperature record from the subpolar North Atlantic constructed using diatoms and statistics and its relation to other climate parameters, *Paleoceanography*, *23*, PA2210, doi:10.1029/2006PA001339.
- Berner, K. S., N. Koç, and F. Godtliobsen (2010), High frequency climate variability of the Norwegian Atlantic Current during the early Holocene period and a possible connection to the Gleissberg cycle, *Holocene*, *20*, 245–255.
- Berner, K. S., N. Koç, F. Godtliobsen, and D. Divine (2011), Holocene climate variability of the Norwegian Atlantic Current during high and low solar insolation forcing, *Paleoceanography*, *26*, PA2220, doi:10.1029/2010PA002002.
- Blaschek, M., P. Bakker, and H. Renssen (2015), The influence of Greenland ice sheet melting on the Atlantic meridional overturning circulation during past and future warm periods: A model study, *Clim. Dyn.*, *44*, 2137–2157.
- Bronk Ramsey, C. (2008), Deposition models for chronological records, *Quat. Sci. Rev.*, *27*, 42–60.
- Bronk Ramsey, C. (2009), Bayesian analysis of radiocarbon dates, *Radiocarbon*, *51*, 337–360.
- Bronk Ramsey, C., and S. Lee (2013), Recent and planned developments of the program OxCal, *Radiocarbon*, *55*, 720–730.
- Cavaliere, D., C. Parkinson, P. Gloersen, and H. J. Zwally (1996), *Sea Ice Concentrations from Nimbus-7 SMMR and DMSP SSM/I-SSMIS Passive Microwave Data*, NASA DAAC at the Natl. Snow and Ice Data Cent., Boulder, Colo.
- Crowley, T. J. (2000), Causes of climate change over the past 1000 years, *Science*, *289*, 270–277.
- Dickson, R. R., J. Meincke, S.-A. Malmberg, and A. J. Lee (1988), The “Great Salinity Anomaly” in the North Atlantic, 1968–1982, *Prog. Oceanogr.*, *20*, 103–151.
- Dickson, R. R., T. J. Osborn, J. W. Hurrell, J. Meincke, J. Blindheim, B. Adlandsvik, T. Vinje, G. Alekseev, and W. Maslowski (2000), The Arctic ocean response to the North Atlantic Oscillation, *J. Clim.*, *13*, 2671–2696.
- Divine, D. V., and D. Dick (2006), Historical variability of sea ice edge position in the Nordic Seas, *J. Geophys. Res.*, *111*, C01001, doi:10.1029/2004JC002851.
- Eddy, J. A. (1978), The Maunder minimum, *Science*, *192*, 1189–1202.
- Eiriksson, J., G. Larsen, K. L. Knudsen, J. Heinemeier, and L. A. Simonarson (2004), Marine reservoir age variability and water mass distribution in the Iceland Sea, *Quat. Sci. Rev.*, *23*, 2247–2268.
- Eiriksson, J., K. L. Knudsen, G. Larsen, J. Olsen, J. Heinemeier, H. B. Bartels-Jónsdóttir, H. Jiang, L. Ran, and L. A. Simonarson (2011), Coupling of palaeoceanographic shifts and changes in marine reservoir ages off North Iceland through the last millennium, *Palaeogeogr. Palaeoclimatol. Palaeoecol.*, *302*, 95–108.
- Goosse, H., E. Crespin, S. Dubinkina, M. F. Loutre, M. E. Mann, H. Renssen, Y. Sallaz-Damaz, and D. Shindell (2012), The role of forcing and internal dynamics in explaining the “Medieval Climate Anomaly”, *Clim. Dyn.*, *39*, 2847–2866.
- Graham, N. E., C. M. Ammann, D. Fleitmann, K. M. Cobb, and J. Luterbacher (2011), Support for global climate reorganization during the “Medieval Climate Anomaly”, *Clim. Dyn.*, *37*, 1217–1245.
- Grinsted, A., J. C. Moore, and S. Jevrejeva (2004), Application of the cross wavelet transform and wavelet coherence to geophysical time series, *Nonlinear Process. Geophys.*, *11*, 561–566.
- Grönvold, K., N. Oskarsson, S. J. Johnsen, H. B. Clausen, C. U. Hammer, G. Bond, and E. Bard (1995), Ash layers from Iceland in the Greenland GRIP ice core correlated with oceanic and land sediments, *Earth Planet. Sci. Lett.*, *135*, 149–155.
- Grove, J. M. (1988), *The Little Ice Age*, pp. 520, Methuen, London.
- Hegerl, G. C., T. J. Crowley, S. K. Baum, K.-Y. Kim, and W. T. Hyde (2003), Detection of volcanic, solar and greenhouse gas signals in paleo-reconstructions of Northern Hemispheric temperature, *Geophys. Res. Lett.*, *30*(5), 1242, doi:10.1029/2002GL016635.

- Jennings, A. E., and G. Helgadottir (1994), Foraminiferal assemblages from the fjords and shelf of Eastern Greenland, *J. Foraminiferal Res.*, *24*, 123–144.
- Jennings, A. E., and N. J. Weiner (1996), Environmental change in eastern Greenland during the last 1300 years: Evidence from foraminifera and lithofacies in Nansen Fjord, 68°N, *Holocene*, *6*, 179–191.
- Jennings, A. E., K. Grønbold, R. Hilberman, M. Smith, and M. Hald (2002), High resolution study of Icelandic tephtras in the Kangerlussuaq Trough, SE East Greenland during the last deglaciation, *J. Quat. Sci.*, *7*, 747–757.
- Jennings, A. E., M. Hald, M. Smith, and J. T. Andrews (2006), Freshwater forcing from the Greenland ice sheet during the Younger Dryas: Evidence from southeastern Greenland shelf cores, *Quat. Sci. Rev.*, *25*, 282–298.
- Jennings, A., J. Andrews, and L. Wilson (2011), Holocene environmental evolution of the SE Greenland Shelf North and South of the Denmark Strait: Irminger and Greenland current interactions, *Quat. Sci. Rev.*, *30*, 980–998.
- Jennings, A., T. Thordarson, K. Zalzal, J. Stoner, C. Hayward, Á. Geirsdóttir, and G. Miller (2014), Holocene tephra from Iceland and Alaska in SE Greenland Shelf Sediments, in *Marine Tephrochronology*, edited by W. E. N. Austin et al., *Geol. Soc. London, Spec. Publ.*, *398*, doi:10.1144/SP398.6.
- Jensen, K. G., A. Kuijpers, N. Koç, and J. Heinemeier (2004), Diatom evidence of hydrographic changes and ice conditions in Igaliku Fjord, South Greenland, during the past 1500 years, *Holocene*, *14*, 152–164.
- Jiang, H., M.-S. Seidenkrantz, K. L. Knudsen, and J. Eiriksson (2001), Diatom surface sediment assemblages around Iceland and their relationship to oceanic environmental variables, *Mar. Micropaleontol.*, *41*, 73–96.
- Jiang, H., J. Eiriksson, M. Schultz, K.-L. Knudsen, and M.-S. Seidenkrantz (2005), Evidence for solar forcing of sea-surface temperature on the North Icelandic Shelf during the Late Holocene, *Geology*, *33*, 73–76.
- Jiang, H., et al. (2015), Solar forcing of Holocene summer sea-surface temperatures in the northern North Atlantic, *Geology*, *43*, 203–206.
- Justwan, A., and N. Koç (2008), A diatom based transfer function for reconstructing sea ice concentrations in the North Atlantic, *Mar. Micropaleontol.*, *66*, 264–278.
- Justwan, A., N. Koç, and A. Jennings (2009), Evolution of the East Greenland Current between 1150 and 1740 AD, revealed by diatom-based sea surface temperature and sea-ice concentration reconstructions, *Polar Res.*, *28*, 165–176.
- Kaufman, D. S., et al. (2009), Recent warming reverses long-term Arctic cooling, *Science*, *325*, 1236–1239.
- Kobashi, T., K. Kawamura, J. P. Severinghaus, J.-M. Barnola, T. Nkaegawa, B. M. Vinther, S. J. Johnsen, and J. E. Box (2011), High variability of Greenland surface temperature over the past 4000 years estimated from trapped air in an ice core, *Geophys. Res. Lett.*, *38*, L21501, doi:10.1029/2011GL049444.
- Koç, N., E. Jansen, and H. Hafliðason (1993), Paleooceanographic reconstruction of surface ocean conditions in the Greenland, Iceland and Norwegian Seas through the last 14 ka based on diatoms, *Quat. Sci. Rev.*, *12*, 115–140.
- Koç-Karpuz, N., and H. Schrader (1990), Surface sediment diatom distribution and Holocene paleo-temperature variations in the Greenland, Iceland and Norwegian Seas through the last 14 ka based on diatoms, *Paleooceanography*, *5*, 557–580.
- Kuijpers, A., N. Mikkelsen, S. Ribeiro, and M.-S. Seidenkrantz (2014), Impact of medieval fjord hydrography and climate on the Western and Eastern Settlements in Norse Greenland, *J. North Atlantic*, *6*, 1–13.
- Lamb, H. H. (1965), The early medieval warm epoch and its sequel, *Palaeogeogr. Palaeoclimatol. Palaeoecol.*, *1*, 13–37.
- Mann, M. E., Z. Zhang, S. Rutherford, R. S. Bradley, M. K. Hughes, D. Shindell, D. C. Ammann, G. Faluvegi, and F. Ni (2009), Global signatures and dynamical origins of the Little Ice Age and Medieval Climate Anomaly, *Science*, *326*, 1256–1260.
- Masse, G., S. J. Rowland, M.-A. Sicre, J. Jacob, E. Jansen, and S. T. Belt (2008), Abrupt climate changes for Iceland during the last millennium: Evidence from high resolution sea ice reconstructions, *Earth Planet. Sci. Lett.*, *269*, 565–569.
- Miettinen, A., N. Koç, I. R. Hall, F. Godtliëbsen, and D. Divine (2011), North Atlantic sea surface temperatures and their relation to the North Atlantic Oscillation during the last 230 years, *Clim. Dyn.*, *36*, 533–543.
- Miettinen, A., D. Divine, N. Koç, F. Godtliëbsen, and I. R. Hall (2012), Multicentennial variability of the sea surface temperature gradient across the subpolar North Atlantic over the last 2.8 kyr, *J. Clim.*, *25*, 4205–4219.
- Miller, G. H., et al. (2012), Abrupt onset of the Little Ice Age triggered by volcanism and sustained by sea-ice/ocean feedbacks, *Geophys. Res. Lett.*, *39*, L02708, doi:10.1029/2011GL050168.
- Moffa-Sánchez, P., A. Born, I. R. Hall, D. J. R. Thornalley, and S. Barker (2014), Solar forcing of North Atlantic surface temperature and salinity over the past millennium, *Nat. Geosci.*, *7*, 275–278.
- Ogilvie, A. E. J. (1996), Sea-ice conditions off the coasts of Iceland A.D. 1601–1850 with special reference to part of the Maunder Minimum period (1675–1715), in *North European Climate Data in the Latter Part of the Maunder Minimum Period A.D. 1675–1715*, edited by E. S. Pedersen, pp. 9–12, Museum of Archaeology, Stravanger AmS-Varia 25, Extended abstracts for the Regional North-European sub-group meeting on historical climatology in Stavanger, Norway.
- Ogilvie, A. E. J., L. K. Barlow, and A. Jennings (2000), North Atlantic climate c. A.D. 1000: Millennial reflections on the Viking discoveries of Iceland, Greenland and North America, *Weather*, *55*, 34–45.
- Olsen, J., N. J. Anderson, and M. F. Knudsen (2012), Variability of the North Atlantic Oscillation over the last 5,200 years, *Nat. Geosci.*, *5*, 808–812.
- Otterå, O. H., M. Bensen, H. Drange, and L. Suo (2010), External forcing as a metronome for Atlantic multidecadal variability, *Nat. Geosci.*, *3*, 688–694.
- Pringle, H. (1997), Death in Norse Greenland, *Science*, *275*, 924–926.
- Ran, L., H. Jiang, K. L. Knudsen, and J. Eiriksson (2011), Diatom-based reconstruction of palaeoceanographic changes on the North Icelandic shelf during the last millennium, *Palaeogeogr. Palaeoclimatol. Palaeoecol.*, *302*, 109–119.
- Reeh, N., H. H. Thomsen, A. K. Higgins, and A. Weidick (2001), Sea ice and the stability of north and northeast Greenland floating glaciers, in *Annals of Glaciology*, vol. 33, edited by M. O. Jeffries and H. Eicken, pp. 474–480, International Glaciological Society, Cambridge.
- Reimer, P. J., et al. (2013), IntCal13 and Marine13 radiocarbon age calibration curves 0–50,000 years cal BP, *Radiocarbon*, *55*, 1869–1887.
- Rudels, B., H. J. Friedrich, and D. Quadfasel (1999), The Arctic Circumpolar Current, *Deep Sea Res., Part II*, 1023–1062.
- Schleussner, C.-F., D. Divine, J. F. Donges, A. Miettinen, and R. Donner (2015), Indications for a North Atlantic Ocean circulation regime shift at the onset of the Little Ice Age, *Clim. Dyn.*, doi:10.1007/s00382-015-2561-x.
- Schrader, H. J., and R. Gersonde (1978), Diatoms and silicoflagellates. Micropaleontological counting methods and techniques—An exercise on an eight meters section of the lower Pliocene of Capo Rossello, *Utrecht Micropaleontol. Bull.*, *17*, 129–176.
- Schulz, M., and M. Mudelsee (2002), REDFIT: Estimating red-noise spectra directly from unevenly spaced paleoclimatic time series, *Comput. Chem.*, *28*, 421–426.
- Schröder, W. (2005), *Case Studies on the Spörer, Maunder, and Dalton Minima*, Science Edition, Bremen.
- Seidenkrantz, M. S., S. Aagaard-Sørensen, H. Sulsbrück, A. Kuijpers, K. G. Jensen, and H. Kunzendorf (2007), Hydrography and climate of the last 4400 years in a SW Greenland, *Holocene*, *17*, 387–401.

- Sha, L., H. Jiang, M.-S. Seidenkrantz, K. L. Knudsen, J. Olsen, A. Kuijpers, and Y. Liu (2014), A diatom-based sea-ice reconstruction for the Vaigat Strait (Disko Bugt, West Greenland) over the last 5000 yr, *Palaeogeogr. Palaeoclimatol. Palaeoecol.*, *403*, 66–79.
- Shindell, D. T., G. A. Schmidt, M. E. Mann, D. Rind, and A. Waple (2001), Solar forcing of regional climate change during the Maunder Minimum, *Science*, *294*, 2149–2152.
- Shindell, D. T., G. Schmidt, R. I. Miller, and M. E. Mann (2003), Volcanic and solar forcing of climate change during the preindustrial era, *J. Clim.*, *16*, 4094–4107.
- Sicre, M.-A., I. R. Hall, J. Mignot, M. Khodri, U. Ezat, M. X. Truong, J. Eiriksson, and K. L. Knudsen (2011), Sea surface temperature variability in the subpolar Atlantic over the last two millennia, *Paleoceanography*, *26*, PA4218, doi:10.1029/2011PA002169.
- Sicre, M.-A., et al. (2014), Labrador Current variability over the last 2000 years, *Earth Planet. Sci. Lett.*, *400*, 26–32.
- Smith, T. M., R. W. Reynolds, T. C. Peterson, and J. Lawrimore (2008), Improvements NOAA's historical merged land–ocean temperature analysis (1880–2006), *J. Clim.*, *21*, 2283–2296.
- Steinhilber, F., et al. (2012), 9,400 years of cosmic radiation and solar activity from ice cores and tree rings, *Proc. Natl. Acad. Sci. U.S.A.*, *109*, 5967–5971.
- Stephens, C., J. I. Antonov, T. P. Boyer, M. E. Conkright, R. A. Locarnini, T. D. O'Brien, and H. E. Garcia (2002), in *World Ocean Atlas 2001, Volume 1: Temperature*, NOAA Atlas NESDIS, vol. 49, edited by S. Levitus, 167 pp., U.S. Gov. Print. Off., Washington, D. C.
- Stoner, J. S., A. Jennings, G. B. Kristjánóttir, G. Dunhill, J. T. Andrews, and J. Hardardóttir (2007), A paleomagnetic approach toward reflecting Holocene radiocarbon based chronologies: Palaeoceanographic records from the north Iceland (MD99-2269) and east Greenland (MD99-2322) margins, *Paleoceanography*, *22*, PA1209, doi:10.1029/2006PA001285.
- Ter-Braak, C. J. F., and S. Juggins (1993), Weighted averaging partial least squares regression (WA-PLS): An improved method for reconstructing environmental variables from species assemblages, *Hydrobiologia*, *269–270*, 485–502.
- Torrence, C., and G. Compo (1998), A practical guide to wavelet analysis, *Bull. Am. Meteorol. Soc.*, *79*, 61–78.
- Trouet, V., J. Esper, N. E. Graham, A. Baker, J. D. Scourse, and D. C. Frank (2009), Persistent positive North Atlantic Oscillation mode dominated the Medieval Climate Anomaly, *Science*, *324*, 78–80.
- Vinther, B. M., P. D. Jones, K. R. Briffa, H. B. Clausen, K. K. Andersen, D. Dahl-Jensen, and S. J. Johnsen (2010), Climatic signals in multiple highly resolved stable isotope records from Greenland, *Quat. Sci. Rev.*, *29*, 522–538.
- von Quillfeldt, C. H. (2001), Identification of some easily confused diatom species in Arctic spring blooms, *Bot. Mar.*, *44*, 375–389.
- Wanner, H., S. Bronnimann, C. Casty, D. Gyalistras, J. Luterbacher, C. Schmutz, D. B. Stephenson, and E. Xoplaki (2001), North Atlantic Oscillation—Concepts and studies, *Surv. Geophys.*, *22*, 321–382.
- Woodgate, R. A., E. Fahrbach, and G. Rohardt (1999), Structure and transport of the East Greenland Current at 75°N from moored current meters, *J. Geophys. Res.*, *104*, 18,059–18,072, doi:10.1029/1999JC900146.
- Xoplaki, E., D. Fleitmann, and H. F. Diaz (2011), Medieval climate anomaly. PAGES news 19, 4.
- Yu, L., Y. Gao, and O. H. Otterø (2015), The sensitivity of the Atlantic meridional overturning circulation to enhanced freshwater discharge along the entire, eastern and western coast of Greenland, *Clim. Dyn.*, doi:10.1007/s00382-015-2651-9.
- Zorita, E., et al. (2010), European temperature records of the past five centuries based on documentary/instrumental information compared to climate simulations, *Clim. Change*, *101*, 143–168.